DEEP-SST-EDDIES: A Deep Learning framework to detect oceanic eddies in Sea Surface Temperature images

Evangelos Moschos, Olivier Schwander, Alexandre Stegner, Patrick Gallinari

DEEP-SST-EDDIES: A DEEP LEARNING FRAMEWORK TO DETECT OCEANIC EDDIES IN SEA SURFACE TEMPERATURE IMAGES

Evangelos Moschos[†] *Olivier Schwander*[⋆] *Alexandre Stegner*[†] *Patrick Gallinari*[⋆‡]

[†] Laboratoire de Météorologie Dynamique (LMD), CNRS-IPSL, École Polytechnique, Palaiseau, France
[⋆]Sorbonne Université, LIP6, Paris, France
[‡] Criteo AI Lab, Paris

ABSTRACT

Until now, mesoscale oceanic eddies have been automatically detected through physical methods on satellite altimetry. Nevertheless, they often have a visible signature on Sea Surface Temperature (SST) satellite images, which have not been yet sufficiently exploited. We introduce a novel method that employs Deep Learning to detect eddy signatures on such input. We provide the first available dataset for this task, retaining SST images through altimetric-based region proposal. We train a CNN-based classifier which succeeds in accurately detecting eddy signatures in well-defined examples. Our experiments show that the difficulty of classifying a large set of automatically retained images can be tackled by training on a smaller subset of manually labeled data. The difference in performance on the two sets is explained by the noisy automatic labeling and intrinsic complexity of the SST signal. This approach can provide to oceanographers a tool for validation of altimetric eddy detection through SST.

Index Terms— Mesoscale Eddies, Oceanography, Sea Surface Temperature, Deep Learning, Remote Sensing

1. INTRODUCTION

Mesoscale eddies are oceanic vortices with horizontal scales on the order of few tens of kilometers and lifetime on the order of weeks or months. These large, coherent structures can trap and transport heat, salt, pollutants and various biogeochemical components from their regions of formation to remote areas [1]. Their dynamics can impact significantly the biological productivity at the ocean surface [2, 3], modify the mixed layer [4], amplify locally the vertical motions [5] and even concentrate and transport microplastics [6]. Thanks to spectacular advances in satellite altimetry, automatic eddy detection and tracking algorithms have become essential analytical tools for studying the dynamics of oceanic eddies.

Plenty of these algorithms, based on multi-satellite altimetry maps, have been developed during the last ten years (we cite some; [7, 8, 9]). These algorithms use geometrical properties of the Sea Surface Height (SSH) field and/or the streamlines of the derived velocity field to detect and track in time vortex structures. However, altimetry satellite products undergo large spatio-temporal interpolation between the areas crossed by satellite tracks, producing low-resolution fields as well as uncertainty in areas which have not been adequately sampled. Recent studies show that many oceanic eddies could be missed or wrongly detected [10].

On the other hand, eddy signatures are also apparent in visible satellite imagery such as Sea Surface Temperature (SST), Ocean Color/Chlorophyll (CHL), or synthetic-aperture radar (SAR images). Even if visible imagery has much higher resolution than altimetry, it may be frequently covered by clouds and the few detection algorithms that have been developed on SST (e.g. [11, 12]) hardly exploit their complex patterns. Deep Learning has been rapidly gaining in popularity and solving problems in remote sensing [13], climate and the environment [14]. Machine learning methods have also been used in previous studies to tackle altimetric eddy detection and tracking on the SSH field via pixel-wise classification [15] or LSTM [16], as well as the velocity field [17]. Albeit their important contributions, they are restricted the limitations of the altimetry field $perse$ (that is, its interpolation) on which the learning dataset is based. Deep learning has also been reportedly employed for classification of eddy signatures in SAR images [18].

In this study we seek to harness the potential of deep learning on the visible satellite imagery of Sea Surface Temperature, which contains high-resolution vortex signatures. To this purpose, we introduce a novel method to obtain a dataset of SST images based on altimetric detection. The SST dataset is available on demand through https://www1.lmd.polytechnique.fr/dyned/data-base.We train a CNN-based classifier which is able to accurately detect eddy signatures on well-defined, manually selected cases. The classifier is tested on a larger set containing noisy labels and shows potential in selecting the accurately labeled images and correcting false labels. This methodology could serve to validate altimetric eddy detection through SST.

Contact:evangelos.moschos@lmd.polytechnique.fr
This study has been conducted using E.U. Copernicus Marine Service Information.

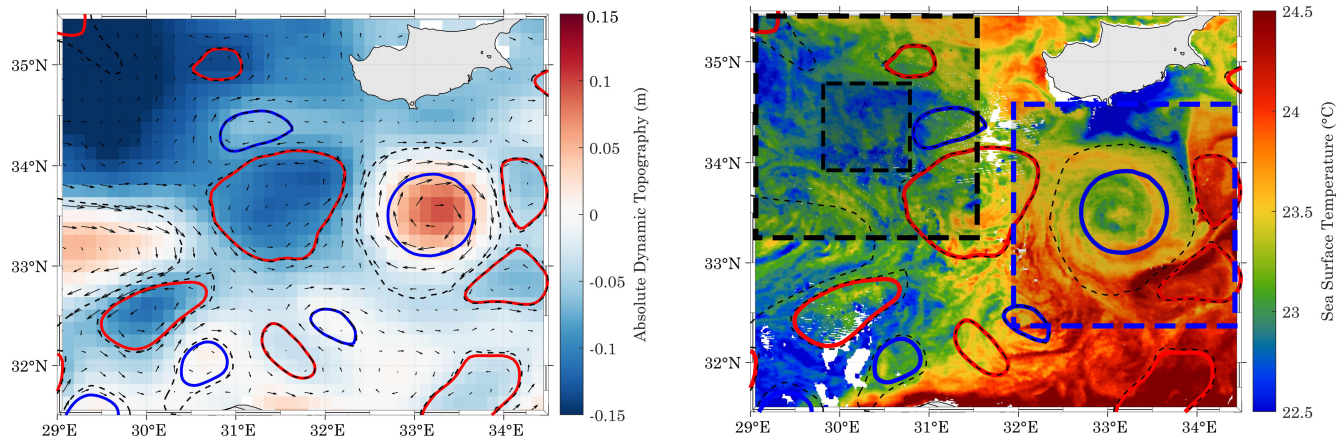

Fig. 1. Altimetric field with superimposed geostrophic velocity vectors (left) and SST field (right) in the Levantine Sea on the 08/06/2017. Maximum velocity contours detected by AMEDA on altimetry are superimposed on both figures. On the rightmost one, the blue box represents a sample AE AoI, the big black box represents a sample NE AoI, and the smaller black box inside it shows the area of no-contour constrain.

2. SST EDDY IMAGE DATASET

2.1. Localizing SST images through altimetric detections

The task of this study consists in classifying SST images which can contain either the signature of an Anticyclonic Eddy (AE), a Cyclonic Eddy (CE) or No Eddy signature (NE). Anticyclones (cyclones) rotate in the opposite (same) direction with the earth's rotation, that is clockwise (counter-clockwise) in the Northern Hemisphere.

To create a data-set of SST images, the Mediterranean Sea is chosen as the domain of study, where through the CMEMS we receive 720 daily high-resolution images for the period of 2016-2017. These images, produced as desribed in [19], consist of of supercollated SST data with a resolution of 1/12° and are representative of night SST values.

To localize and retain Areas of Interest (AoI) containing AE and CE signatures on the SST field, we utilize the daily outputs of the Angular Momentum Eddy Detection and tracking Algorithm ($AMEDA$) [9], working on satellite altimetry and applied on the AVISO/DUACS field of geostrophic velocities. The AMEDA detects eddies by identifying minima and maxima on the geostrophic velocity field and selecting closed streamlines around them. The algorithm does also dynamically track eddies backward and forward in time, as well as identifies their merging and splitting events. Eddy tracks detected by AMEDA, labeled as AE or CE based on their sense of rotation, with information on the closed contour of maximum velocity and other properties, are contained in the DYNED-Atlas [1]

[1]The DYNED-Atlas, containing more than 11500 eddy tracks for the 2000-2017 period in the Mediterranean Sea, is publicly available through: https://www1.lmd.polytechnique.fr/dyned/data-base

For each day of the two-year period of study, we co-localize the AE and CE contours received from AMEDA with the SST images both referring to the domain of the Med Sea. In this sense, physical detections on altimetry act as a region proposal for class-representative SST image extraction. Around each AMEDA contour we crop a AoI with side $k = \lambda * R_{max}$ where R_{max} is the radius of a circle of equivalent area with the AMEDA maximum velocity contour, and $\lambda = 5$. These AoI are interpolated to a constant size of $m = \lambda * \bar{R}_{max}(km)$ where $\bar{R}_{max} = 42.5km$ is the mean maximum velocity radius of all AMEDA contours retained, resulting in an image size of $m = 230$ pixels. In order to receive SST images labeled as NE, that is, not containing an eddy signature, an AoI of size $m = 230$ pixels is slided along the domain of the Mediterranean Sea. AoI that do not contain any AMEDA contour in their center (in a smaller box of side R_{max}) are retained as NE images. The above methodology is visualized in Figure 1.

All the retained images are also furtherly filtered based on the altimetric satellite track coverage of the AoI and the cloud coverage of the SST image. Thus SST images corresponding to altimetric detections with the lowest uncertainty are selected. A threshold of 50% is selected as the maximum missing values due to clouds for an image to be retained.

2.2. Dataset features and labels

We automatically retain a dataset of SST images with 4000 images for each of the AE,CE and NE classes (total of 12000 images). These are one-channel images with values that represent the grid temperature in degrees Celsius.

Examples of images contained in the Dataset are given in Figure 2. They are distincted based on whether they contain

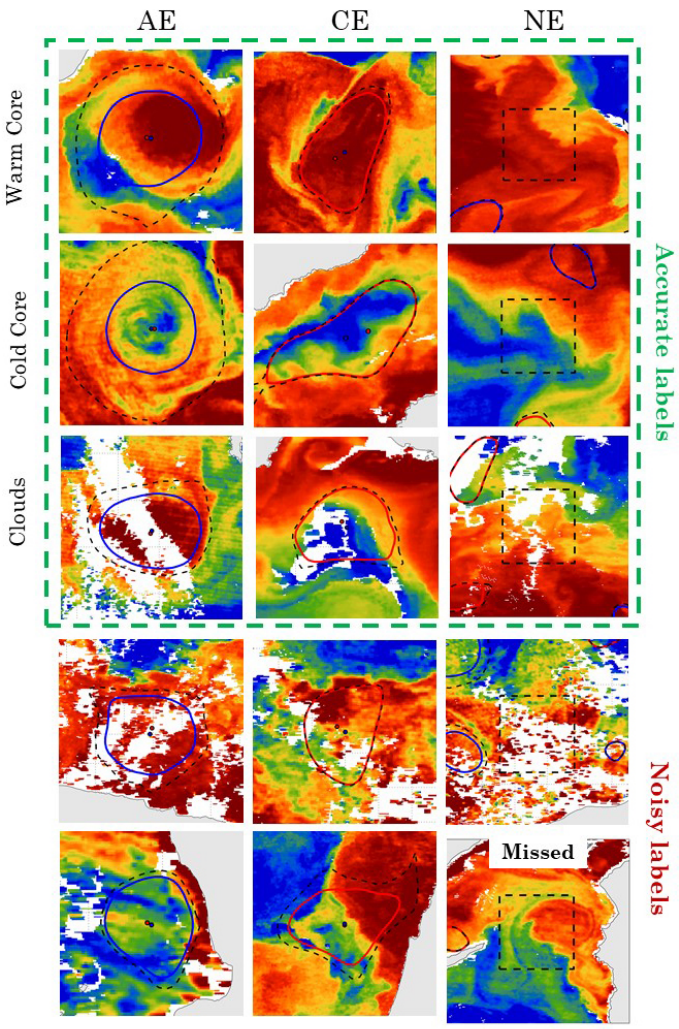

Fig. 2. Samples of SST images, plotted together with the AMEDA contours. Columns represent the three classes. Dashed line boxes on NE images represent the areas of no-contour constrain. Examples with both accurate and noisy labels are given. Colours represent one channel images in a perceptually uniform jet colormap between the 5th and the 95th percentile of the image range of temperature values. Clouds are visualized with white colour and land with a gray patch.

an eddy signature (AE, CE) or not (NE). Apart from their sense of rotation, eddy signature images can also be visually characterized by the sign of their core anomaly: both warm and cold core cases exist for the two classes AE and CE.

In order to enhance feature extraction and generalization, two methods are followed: The first consists of applying rotational augmentation during the training process. This way, rotational invariance, on images which depict physically rotating structures, can be learned. The second concerns cloud coverage: all cloud cover pixels are set to zero value. An extra channel of a semantic mask is added to each image, where all non cloud points are set to a value of one.

Setup	Test Accuracy
EDDIES-HL	92.9 ± 1.3 %
EDDIES-HL (+Mask)	93.8 ± 1.1 %
EDDIES-HL (+Rotation)	94.7 ± 1.0
EDDIES-HL (+Mask+Rot)	95.6 ± 0.5 %

Table 1. Test accuracy for different setups on the EDDIES-HL dataset training. Reported scores are means $\pm$ stdev, of the 5-fold cross validation.

Noisy labels are contained in the Dataset: images selected through AMEDA contours and labeled as AE or CE might not contain eddy signature or, *mutatis mutandis*, images labeled as NE might contain the signature of an eddy missed by AMEDA. Mislabeling by AMEDA can be due to intrinsic limits of the altimetric dataset or algorithm errors. Cloud coverage and air-sea processes can also affect significantly the surface eddy signature. Through visual sampling of the automatically received, noisy labeled, Dataset, we diagnose a 20% of images being accurately labeled and a 80% containing false or uncertain labels. Because of this effect we manually separate 1,200 images (400 per class) creating a of handpicked, accurate labeled (here on $EDDIES-HL$) and class-representative examples. From the total Dataset we remove the images contained in the EDDIES-HL dataset to receive a large dataset of 10,8000 images containing noisy labels (here on $EDDIES-AUTO$).

3. TRAINING A CNN-BASED CLASSIFIER

Convolutional Neural Networks have been exceptionally successful in practical applications which consist of processing complex imagery, as is the case of the satellite data used here. A CNN-based classifier is employed to treat the 3-class problem, using a Cross-Entropy Loss, Stochastic Gradient Descent with momentum and a SoftMax output. Residual Networks [20] use skip connections between layers in order to build efficient Deep Architectures. A pretrained ResNet18 architecture is used in this study, downloaded through the torchvision package of the Pytorch library. All 18 layers are finetuned during the training process.

Apart from the test set, a validation set (consisting of 10% of the train set) is used in our experiments. This allows early stopping based on loss function convergence to a local minimum with a certain patience, in order to avoid overfitting.

4. RESULTS AND DISCUSSION

A 5-fold stratified cross validation is performed through a 80/20 train/test split on the EDDIES-HL dataset. For four

different setups, the mean and standard deviation of the accuracy on the test set, is shown on Table 1. The positive effect of adding a semantic mask and a rotation is seen through the increase in mean accuracy and decrease in divergence of models trained on different folds.

For a more in depth view of model performance, the normalized confusion matrix on the EDDIES-HL set (using both the semantic mask and rotational augmentation techniques) is plotted in Figure 3(a). An overall accuracy of 95.6% is achieved, with a good convergence between different folds ($\sigma = 0.5\%$). The high precision on the AE denotes the prevalence of clear signatures in anticyclonic images. Also the zero misspredictions between AE and CE classes depicts the ability of our model to clearly separate between eddy signature classes. The model shows small error in discriminating CE images from NE. This can be explained by the fact that cyclonic signatures are in general weaker on SST than anticyclonic ones.

The performance of the models trained on the EDDIES-HL dataset is then evaluated on the EDDIES-AUTO dataset. The results of the confusion matrix in Figure 3(b) shows the difference between the label predicted by the model and the (noisy) label of this dataset. The drop in accuracy here, is caused by the false labels as well as the larger variance of features (increased cloud coverage and unclear signatures) of the images contained in EDDIES-AUTO. Nevertheless, the model is still able to separate clearly the AE from CE signatures.

In Figure 3(c) some characteristic examples of the above matrix are visualized, illustrating the ability of the model to predict physically accurate labels on noisy labeled images. Samples outside of the diagonal are examples of false label corrections. The confidence of the model is also evaluated by visually inspecting 400 correctly predicted images per class, above a score threshold of $t = 0.90$. Of them 90% of AE, 70% of CE and 95% of NE have a visual signal corresponding to their predicted label. The model trained on the well-defined samples shows therefore robust performance in selecting the accurately labeled AE and NE images among the noisy labeled ones, which could be used to further enlarge the EDDIES-HL dataset in a semi-supervised learning fashion. Performance is less reliable for the CE class, depicting that the signature of cyclones on SST is more complex and difficult to distinguish.

5. CONCLUSION AND PERSPECTIVES

In this study classification of mesoscale oceanic eddy signatures in Sea Surface Temperature Images is introduced. A methodology is presented to automatically obtain a dataset of SST images, using region proposal provided by physical detections on the altimetric field. An accuracy of 95.6 ± 0.5 is performed on a manually selected dataset of 1200 images with accurate labels (EDDIES-HL), by finetuning a pretrained

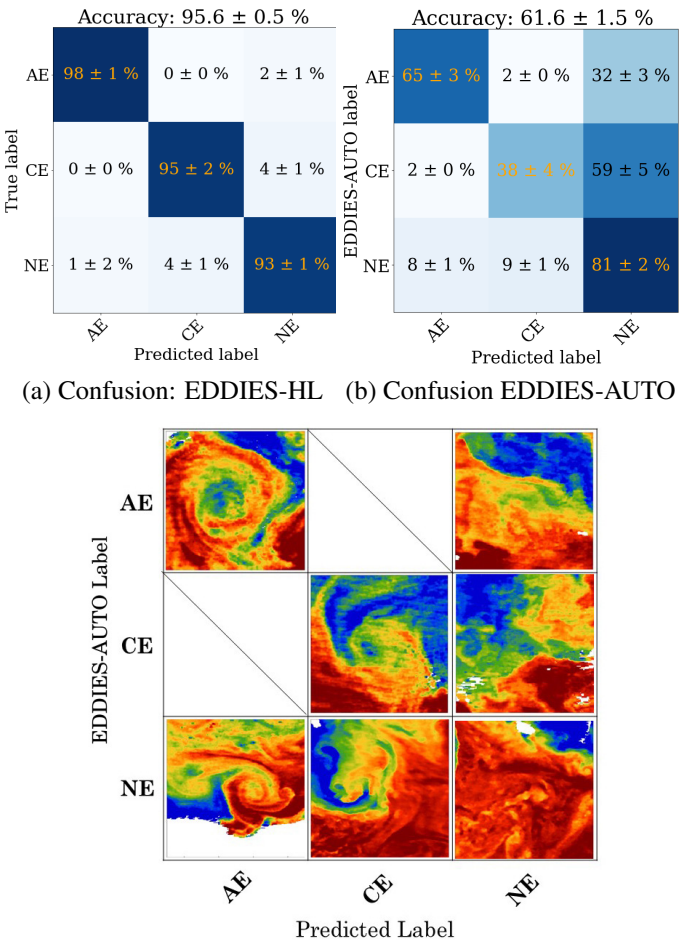

(a) Confusion: EDDIES-HL (b) Confusion EDDIES-AUTO

(c) Samples from EDDIES-AUTO confusion matrix

Fig. 3. (a-b): Normalized Confusion Matrices of the model trained with a 5-fold cross validation on the EDDIES-HL dataset and tested on the two different datasets. (c): Characteristic samples corresponding to cells of the matrix in (b).

ResNet18. The same network is tested on a larger dataset with noisy labels (EDDIES-AUTO) in order to evaluate its ability to select among them those accurately labeled, and correct false labels. Our CNN-based classifier shows robust performance in detecting Anticyclonic Eddy signatures in images and a less reliable one in detecting Cyclonic Eddy signatures.

In future work, methods used for treating and correcting noisy labels [21, 22, 23] can be utilized to self-learn on a large dataset of noisy-labeled images guided through a dataset of accurate labeled ones. Ultimately, object detection and tracking methods as in [24, 25] could be applied on multi-modal images containing eddy signatures, harnessing the power of deep learning to surpass the limits of altimetric eddy detection.

6. REFERENCES

[1] Zhengguang Zhang, Wei Wang, and Bo Qiu, "Oceanic mass transport by mesoscale eddies," *Science*, vol. 345, no. 6194, pp. 322–324, 2014.

[2] Peter Gaube, Dudley B Chelton, Peter G Strutton, and Michael J Behrenfeld, "Satellite observations of chlorophyll, phytoplankton biomass, and ekman pumping in nonlinear mesoscale eddies," *Journal of Geophysical Research: Oceans*, vol. 118, no. 12, pp. 6349–6370, 2013.

[3] Dennis J McGillicuddy Jr, "Mechanisms of physical-biological-biogeochemical interaction at the oceanic mesoscale," *Annual Review of Marine Science*, vol. 8, pp. 125–159, 2016.

[4] Shinya Kouketsu, Hiroyuki Tomita, Eitarou Oka, Shigeki Hosoda, Taiyo Kobayashi, and Kanako Sato, "The role of meso-scale eddies in mixed layer deepening and mode water formation in the western north pacific," in *New Developments in Mode-Water Research*, pp. 59–73. Springer, 2011.

[5] Patrice Klein and Guillaume Lapeyre, "The oceanic vertical pump induced by mesoscale and submesoscale turbulence," *Annual review of marine science*, vol. 1, pp. 351–375, 2009.

[6] Laurent Brach, Patrick Deixonne, Marie-France Bernard, Edmée Durand, Marie-Christine Desjean, Emile Perez, Erik van Sebille, and Alexandra ter Halle, "Anticyclonic eddies increase accumulation of microplastic in the north atlantic subtropical gyre," *Marine pollution bulletin*, vol. 126, pp. 191–196, 2018.

[7] Francesco Nencioli, Changming Dong, Tommy Dickey, Libe Washburn, and James C McWilliams, "A vector geometry–based eddy detection algorithm and its application to a high-resolution numerical model product and high-frequency radar surface velocities in the southern california bight," *Journal of Atmospheric and Oceanic Technology*, vol. 27, no. 3, pp. 564–579, 2010.

[8] Dudley B Chelton, Michael G Schlax, and Roger M Samelson, "Global observations of nonlinear mesoscale eddies," *Progress in Oceanography*, vol. 91, no. 2, pp. 167–216, 2011.

[9] Briac Le Vu, Alexandre Stegner, and Thomas Arsouze, "Angular momentum eddy detection and tracking algorithm (ameda) and its application to coastal eddy formation," *Journal of Atmospheric and Oceanic Technology*, vol. 35, no. 4, pp. 739–762, 2018.

[10] Angel Amores, Gabriel Jordà, Thomas Arsouze, and Julien Le Sommer, "Up to what extent can we characterize ocean eddies using present-day gridded altimetric products?," *Journal of Geophysical Research: Oceans*, vol. 123, no. 10, pp. 7220–7236, 2018.

[11] Davide D'Alimonte, "Detection of mesoscale eddy-related structures through iso-sst patterns," *IEEE Geoscience and Remote Sensing Letters*, vol. 6, no. 2, pp. 189–193, 2009.

[12] Changming Dong, Francesco Nencioli, Yu Liu, and James C McWilliams, "An automated approach to detect oceanic eddies from satellite remotely sensed sea surface temperature data," *IEEE Geoscience and Remote Sensing Letters*, vol. 8, no. 6, pp. 1055–1059, 2011.

[13] Liangpei Zhang, Lefei Zhang, and Bo Du, "Deep learning for remote sensing data: A technical tutorial on the state of the art," *IEEE Geoscience and Remote Sensing Magazine*, vol. 4, no. 2, pp. 22–40, 2016.

[14] David Rolnick, Priya L Donti, Lynn H Kaack, Kelly Kochanski, Alexandre Lacoste, Kris Sankaran, Andrew Slavin Ross, Nikola Milojevic-Dupont, Natasha Jaques, Anna Waldman-Brown, et al., "Tackling climate change with machine learning," *arXiv preprint arXiv:1906.05433*, 2019.

[15] Redouane Lguensat, Miao Sun, Ronan Fablet, Pierre Tandeo, Evan Mason, and Ge Chen, "Eddynet: A deep neural network for pixel-wise classification of oceanic eddies," in *IGARSS 2018-2018 IEEE International Geoscience and Remote Sensing Symposium*. IEEE, 2018, pp. 1764–1767.

[16] Katharina Franz, Ribana Roscher, Andres Milioto, Susanne Wenzel, and Jürgen Kusche, "Ocean eddy identification and tracking using neural networks," in *IGARSS 2018-2018 IEEE International Geoscience and Remote Sensing Symposium*. IEEE, 2018, pp. 6887–6890.

[17] Mohammad D Ashkezari, Christopher N Hill, Christopher N Follett, Gaël Forget, and Michael J Follows, "Oceanic eddy detection and lifetime forecast using machine learning methods," *Geophysical Research Letters*, vol. 43, no. 23, pp. 12–234, 2016.

[18] Dongmei Huang, Yanling Du, Qi He, Wei Song, and Antonio Liotta, "Deepeddy: A simple deep architecture for mesoscale oceanic eddy detection in sar images," in *2017 IEEE 14th International Conference on Networking, Sensing and Control (ICNSC)*. IEEE, 2017, pp. 673–678.

[19] B Buongiorno Nardelli, C Tronconi, A Pisano, and R Santoleri, "High and ultra-high resolution processing of satellite sea surface temperature data over southern european seas in the framework of myocean project," *Remote Sensing of Environment*, vol. 129, pp. 1–16, 2013.

[20] Kaiming He, Xiangyu Zhang, Shaoqing Ren, and Jian Sun, "Deep residual learning for image recognition," in *Proceedings of the IEEE conference on computer vision and pattern recognition*, 2016, pp. 770–778.

[21] Volodymyr Mnih and Geoffrey E Hinton, "Learning to label aerial images from noisy data," in *Proceedings of the 29th International conference on machine learning (ICML-12)*, 2012, pp. 567–574.

[22] Sainbayar Sukhbaatar, Joan Bruna, Manohar Paluri, Lubomir Bourdev, and Rob Fergus, "Training convolutional networks with noisy labels," *arXiv preprint arXiv:1406.2080*, 2014.

[23] Curtis G Northcutt, Lu Jiang, and Isaac L Chuang, "Confident learning: Estimating uncertainty in dataset labels," *arXiv preprint arXiv:1911.00068*, 2019.

[24] Shaoqing Ren, Kaiming He, Ross Girshick, and Jian Sun, "Faster r-cnn: Towards real-time object detection with region proposal networks," in *Advances in neural information processing systems*, 2015, pp. 91–99.

[25] Luca Bertinetto, Jack Valmadre, Joao F Henriques, Andrea Vedaldi, and Philip HS Torr, "Fully-convolutional siamese networks for object tracking," in *European conference on computer vision*. Springer, 2016, pp. 850–865.